



CARD14 Gain-of-Function Mutation Alone Is Sufficient to Drive IL-23/IL-17–Mediated Psoriasiform Skin Inflammation In Vivo

Mark Mellett^{1,4}, Barbara Meier¹, Deepa Mohanan¹, Rebekka Schairer², Phil Cheng¹, Takashi K. Satoh¹, Betina Kiefer¹, Caroline Ospelt³, Stephan Nobbe¹, Margot Thome², Emmanuel Contassot¹ and Lars E. French^{1,4}

Rare autosomal dominant mutations in the gene encoding the keratinocyte signaling molecule CARD14, have been associated with an increased susceptibility to psoriasis, but the physiological impact of CARD14 gain-of-function mutations remains to be fully determined in vivo. Here, we report that heterozygous mice harboring a CARD14 gain-of-function mutation (*Card14* Δ E138) spontaneously develop a chronic psoriatic phenotype with characteristic scaling skin lesions, epidermal thickening, keratinocyte hyperproliferation, hyperkeratosis, and immune cell infiltration. Affected skin of these mice is characterized by elevated expression of anti-microbial peptides, chemokines, and cytokines (including T helper type 17 cell-signature cytokines) and an immune infiltrate rich in neutrophils, myeloid cells, and T cells, reminiscent of human psoriatic skin. Disease pathogenesis was driven by the IL-23/IL-17 axis, and neutralization of IL-23p19, the key cytokine in maintaining T helper type 17 cell polarization, significantly reduced skin lesions and the expression of antimicrobial peptides and proinflammatory cytokines. Therefore, hyperactivation of CARD14 alone is sufficient to orchestrate the complex immunopathogenesis that drives T helper type 17-mediated psoriasis skin disease in vivo.

Journal of Investigative Dermatology (2018) **138**, 2010–2023; doi:10.1016/j.jid.2018.03.1525

INTRODUCTION

Psoriasis is a common chronic inflammatory disease of the skin that is estimated to affect approximately 2% of the global population and is equally prevalent in males and females (Christophers, 2001; Gudjonsson and Elder, 2007). Psoriasis is characterized by scaly erythematous plaques on the skin, which, given its chronic course, significantly impairs the quality of life of affected individuals. The most common form of psoriasis is psoriasis vulgaris (plaque psoriasis), but other forms exist with distinct clinical features, including guttate psoriasis, pustular psoriasis, and palmoplantar psoriasis (Griffiths and Barker, 2007). Overall, 20–30% of plaque psoriasis cases are associated with debilitating psoriatic arthritis, and psoriasis patients can suffer from comorbidities including cardiovascular disease, diabetes, and obesity (Griffiths and Barker, 2007; Mease et al., 2013). Histological hallmarks of psoriasis include epidermal acanthosis, keratinocyte hyperproliferation, hyperkeratosis, cutaneous immune

cell infiltration, and angiogenesis. Disease symptoms arise from a complex interaction between keratinocytes and infiltrating immune cells (Bos and De Rie, 1999; Boyman et al., 2007; Sano et al., 2005; Valdimarsson et al., 1995). However, the early triggers that lead to full-blown disease are not well understood, confounded by the wide range of genetic factors that contribute to an elevated risk of developing psoriasis, including genes controlling epidermal barrier integrity (e.g., *LCE3B*, *LCE3D*) and antigen presentation (e.g., *HLA-Cw*0602*, *ERAP1*) and genes of the innate (e.g., *NFKBIA*) and adaptive immune systems (e.g., *IL12B*, *IL23R*) (Tsoi et al., 2012). Although genome-wide association studies have shown that approximately more than 80 genes in Caucasian and Han Chinese populations are associated with an increased susceptibility to psoriasis, very few genetic variants have actually been studied in vivo (Sheng et al., 2014; Tsoi et al., 2017).

Rare autosomal dominant mutations in the gene encoding a keratinocyte scaffold molecule, CARD14 (which maps to the *PSORS2* locus) have been associated with a number of psoriatic phenotypes including plaque psoriasis and psoriatic arthritis, generalized pustular psoriasis, and palmoplantar pustular psoriasis, in addition to familial and sporadic cases of the clinically related but rare disease pityriasis rubra pilaris (PRP) (Fuchs-Telem et al., 2012; Has et al., 2016; Hong et al., 2014; Jordan et al., 2012a, 2012b; Li et al., 2015; Mossner et al., 2015; Sugiura et al., 2014; Takeichi et al., 2017a, 2017b). CARD14 is a proinflammatory signaling molecule whose expression is predominantly restricted to the placenta and keratinocytes of the skin, although CARD14 expression was also reported on CD31-positive endothelial cells (Fuchs-Telem, 2012; Harden et al., 2014). CARD14 is the second

¹Department of Dermatology, University Hospital of Zürich, Zürich, Switzerland; ²Department of Biochemistry, Center of Immunity and Infection, University of Lausanne, Epalinges, Switzerland; and ³Department of Rheumatology, University Hospital of Zürich, Zürich, Switzerland

⁴These authors contributed equally to this work as co-senior authors.

Correspondence: Mark Mellett, Dermatology Department, University Hospital Zürich, Switzerland. E-mail: mark.mellett@usz.ch or Lars E. French, Dermatology Department, University Hospital Zürich, Switzerland. E-mail: lars.french@uzh.ch

Abbreviations: CARMA, CARD/MAGUK domain; GoF, gain of function; PRP, pityriasis rubra pilaris; Th, T helper; WT, wild type

Received 18 December 2017; revised 22 March 2018; accepted 27 March 2018; accepted manuscript published online 22 April 2018; corrected proof published online 20 July 2018

member of the CARD/MAGUK domain (CARMA) protein family (Bertin et al., 2001; Scudiero et al., 2014). CARMA proteins contain CARD, coiled-coil, SH3, and guanylate kinase-like domains, and they exist in an auto-inhibitory state. In response to external stimuli, CARMA proteins are phosphorylated via protein kinase C isoforms (Scudiero et al., 2014). Subsequently, they undergo a conformational change, facilitating recruitment of the interacting partners Bcl10 (via CARD:CARD domain interactions) and Malt1 to form the CARMA:Bcl10:Malt1 (i.e., CBM) signaling complex, or “signalosome” (Bertin, 2001; Gaide et al., 2001; Howes et al., 2016; Jattani et al., 2016; McAllister-Lucas et al., 2001; Scudiero, 2014). CARD11 (CARMA1), expressed in lymphoid cells, is activated upon B- and T-cell receptor engagement, and gain-of-function (GoF) mutations in the genes encoding CARD11, Bcl10, and Malt1 have been associated with a number of lymphoid malignancies (Gaide, et al., 2002; Juilland and Thome, 2016; Pomerantz et al., 2002; Wang et al., 2002). Similarly, CARD10 (CARMA3), expressed in epithelial tissue and activated by G protein-coupled receptor stimulation, has been linked to the progression of various carcinomas (Du et al., 2014; Pan et al., 2016; Xia et al., 2016; Xie et al., 2014).

CARD14 was recently described to be activated in vitro in response to zymosan and *Staphylococcus aureus* pathogen-associated molecular pattern agonists (Schmitt et al., 2016; Scudiero et al., 2017). Therefore, CARD14 likely plays its main role in innate immune defense, which is supported by the genes activated downstream of CARD14, which typically encode for proinflammatory cytokines and chemokines, including IL-36 γ , IL-8, and Ccl20 (Jordan, 2012a). The contribution of CARD14 GoF to psoriatic disease pathogenesis, however, remains unclear. CARD14 mutations are rare, and some polymorphisms (p.Arg820Trp, p.Arg547Ser) associated with PRP in a Taiwanese study were also shown to be present in the general population (Hong, 2014). Other polymorphisms (p.Gly117Ser) have shown phenotypes that vary considerably, with respect to age of onset and severity, raising the possibility that other genetic or environmental factors may be required (Jordan, 2012b).

Mutation or deletion of a single glutamic acid (E138) in the coiled-coil domain of CARD14 has been associated with both psoriasis and PRP (Fuchs-Telem, 2012; Has, 2016; Inoue et al., 2016; Jordan, 2012b). These variants resulted in severe phenotypes and add support to the relevance of CARD14 mutations to an increased risk of psoriatic skin disease. However, the contribution of CARD14 to psoriasis pathogenesis remains open, and therefore we sought to determine the functional impact of CARD14 E138 mutation in vivo.

RESULTS

CARD14 GoF mutation causes spontaneous signalosome formation in primary human keratinocytes, which is dependent on a functional CARD domain

Consistent with previous reports, CARD14 E138A and Δ E138 mutants both caused enhanced NF- κ B and AP-1 activation in vitro in HEK293 cells compared with wild-type (WT) CARD14, with the E138A mutant showing a more potent response (see Supplementary Figure S1a online) (Afonina et al., 2016; Li et al., 2015). CARD14 E138A and CARD14

Δ E138 GoF mutants were also overexpressed in primary keratinocytes and HEK293 cells and were observed to interact with endogenous Bcl10 by co-immunoprecipitation (Figure 1a, and see Supplementary Figure S1b), whereas Bcl10 interaction with CARD14 WT was below detectable levels. Because this was contrary to previous findings (Afonina, 2016; Scudiero, 2011), we sought to assess other means of CARD14 activity. There was a reduction of Bcl10 expression observed in the presence of all three CARD14 constructs in HEK293 cells (see Supplementary Figure S1b) and a decrease of CARD14 mutant expression in primary keratinocytes (Figure 1a). Previously, it has been suggested that CARD14 mutants associated with psoriasis are less soluble than WT CARD14 (Berki et al., 2015). Additionally, it has been previously described that Bcl10 forms oligomeric structures that can be nucleated by CARD11 (Qiao et al., 2013). It was therefore of interest to determine whether interaction of CARD14 with Bcl10 can induce nucleation and insolubility of the latter. First, we assessed whether mutation of the CARD14 CARD domain could diminish downstream effects. The CARD14 R38 residue has been previously described to be at the Bcl10-interacting interface, and substitution of arginine R38 with cysteine in the CARD domain was previously reported to lack the ability to activate NF- κ B (Jordan, 2012b; Qiao, 2013); therefore, it was anticipated that the R38C mutation would abolish CARD:CARD interactions. Indeed, mutation of the R38 residue in the CARD14 E138A construct completely abrogates the ability of the E138A mutant to interact with Bcl10 (see Figure 1b, Supplementary Figure S1c) and to potentially activate NF- κ B and AP-1 in HEK293 cells (see Supplementary Figure S1d). R38C mutation also diminished the ability of CARD14 E138A to drive IL-8 production in primary keratinocytes (see Supplementary Figure S1e).

To assess nucleation of Bcl10 in the presence of CARD14 GoF mutants, primary keratinocytes were transfected with CARD14 WT, CARD14 E138A, and CARD14 R38C/E138A. Cells were lysed in Triton X-100-containing buffer (Sigma Aldrich, St. Louis, MI), and Triton-insoluble and soluble fractions were assessed by SDS-PAGE. As expected, mutant CARD14 variants were found at higher levels in the insoluble fraction than WT CARD14. Moreover, levels of Bcl10 were more highly increased in the insoluble fraction in the presence of CARD14 E138A compared with CARD14 WT, and this was dependent on a functional CARD domain (Figure 1c), also consistent with a previous report (Bertin et al., 2001).

Insoluble mutant CARD14 E138A and CARD14 Δ E138/Bcl10 complexes or “signalosomes” are visible by confocal microscopy in primary keratinocytes (Figure 1d), whereas CARD14 WT was more widely expressed throughout the cytoplasm, consistent with its weak interaction with Bcl10 in co-immunoprecipitation studies. CARD14 R38C/E138A retained the ability to form insoluble oligomers (Figure 1c and d), but it failed to recruit Bcl10 to these complexes in primary keratinocytes (Figure 1d).

Spontaneous signalosome formation induced by CARD14 E138A and CARD14 Δ E138 resulted in enhanced Malt1 para-caspase activity in HEK293 cells, as measured using a previously described fluorescence resonance energy transfer-

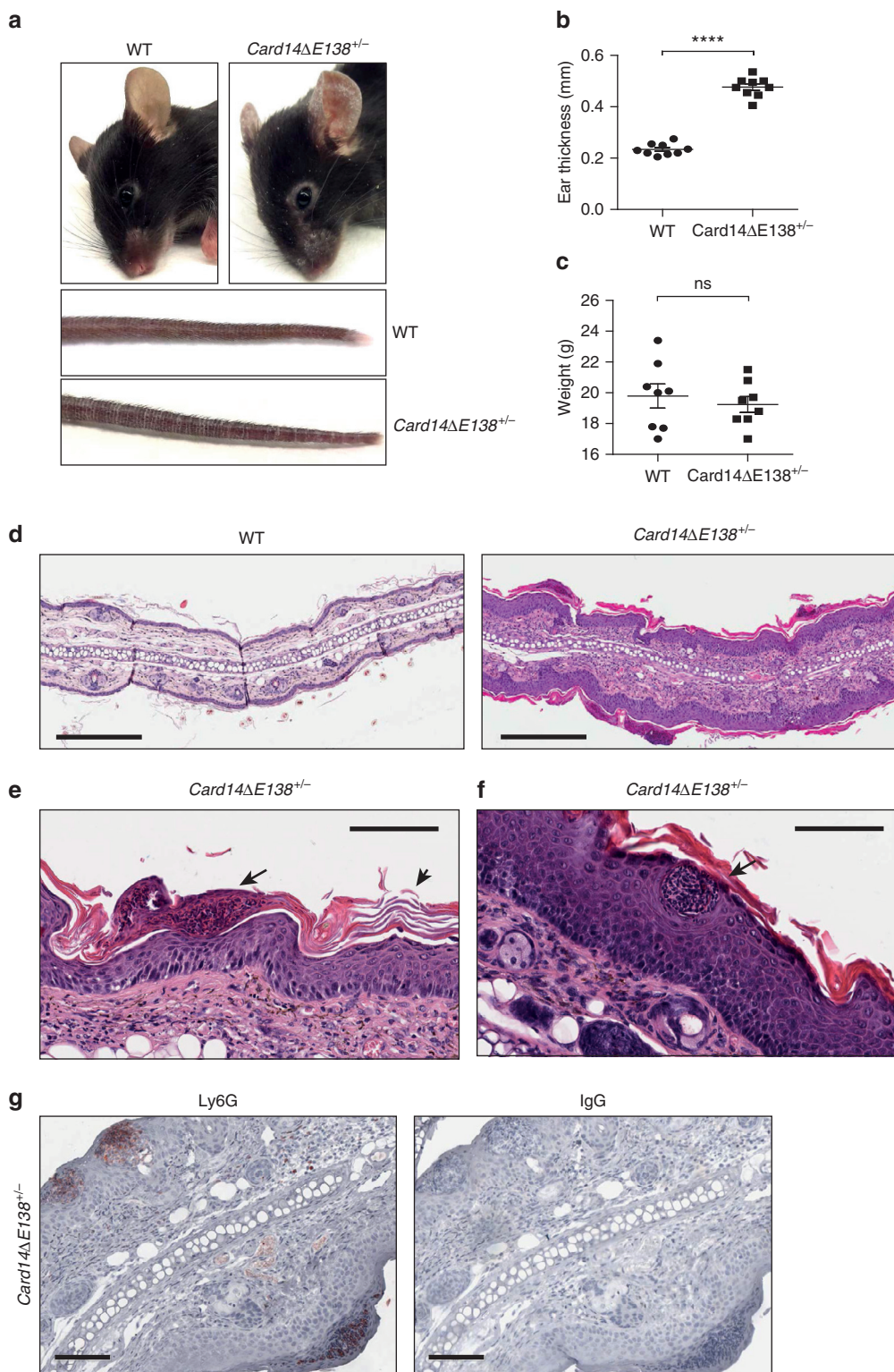


Figure 2. *Card14ΔE138^{+/-}* heterozygous mice develop a spontaneous psoriatic phenotype.

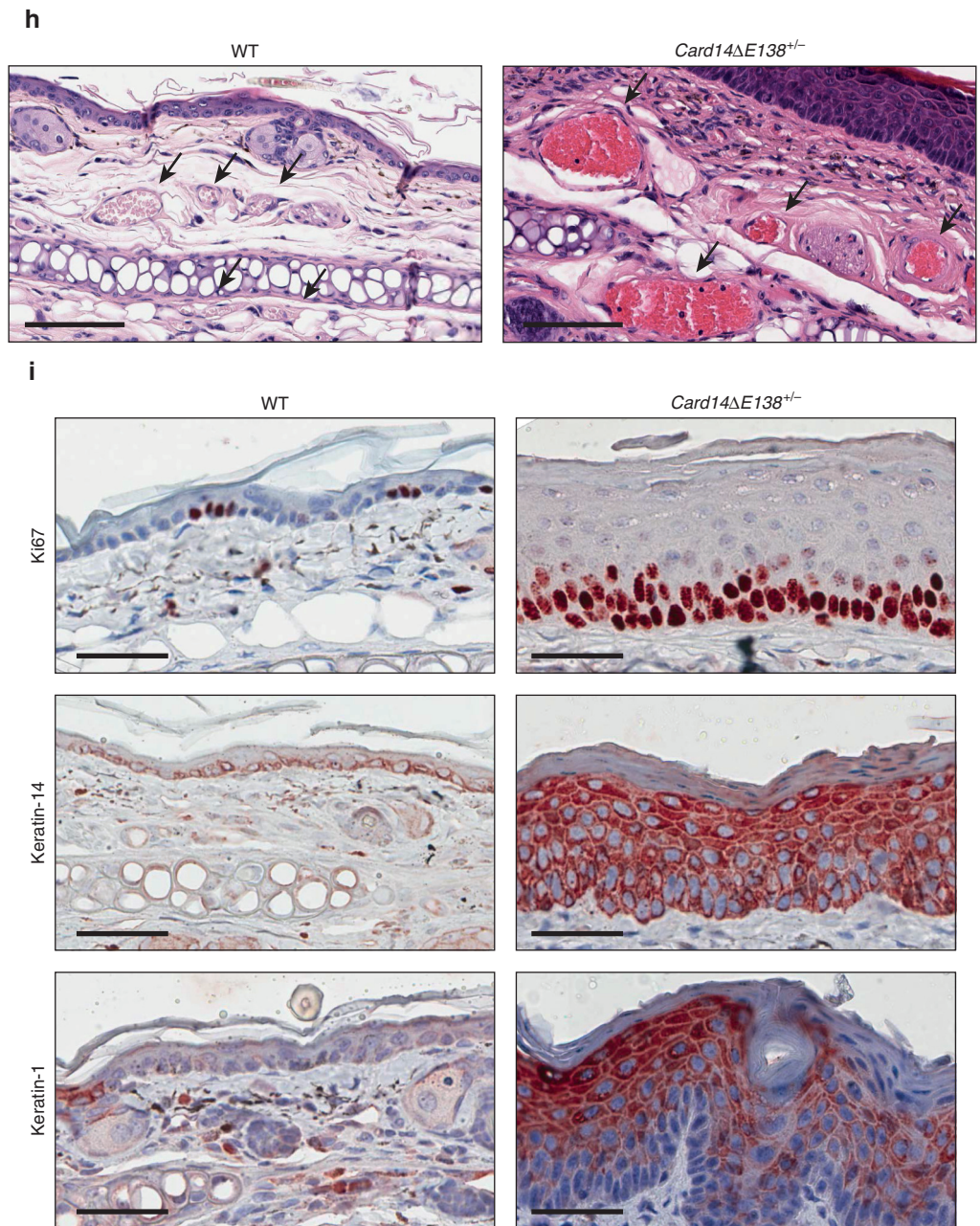
(a) 8-week-old *Card14ΔE138^{+/-}* heterozygous mice develop dry skin around the eyes and whiskers and dry flaky skin on the ears and tail. (b) Ear thickness (mm) of *Card14ΔE138^{+/-}* and wild-type littermates measured with microcalipers (n = 9 per group). (c) *Card14ΔE138^{+/-}* mice and wild-type littermates were weighed at 8 weeks old (n = 8 per group). (d–f, h) Hematoxylin and eosin staining of ear sections from 8-week-old *Card14ΔE138^{+/-}* and wild-type mice. Arrows show (e) parakeratosis (arrow) and orthokeratosis (arrowhead), (f) microabscess, and (h) blood vessels. Scale bar = 300 μm in d or 100 μm in e, f, and h. (g) Ear sections from 8-week-old *Card14ΔE138^{+/-}* mice stained with a specific anti-Ly6G antibody or isotype control. Scale bar = 100 μm. (i) Ear sections from 8-week-old *Card14ΔE138^{+/-}* and wild-type littermates were stained with specific antibodies against Ki67, keratin-14, and keratin-1. Images (a) are representative of all *Card14ΔE138^{+/-}* heterozygous mice observed or (d–i) are representative of 8 individual mice per group, or (b, c) each data point represents an individual mouse and was subjected to a two-tailed unpaired Student *t* test, *****P* < 0.0001. ns, nonsignificant; WT, wild type.

based assay (Pelzer et al., 2013) (Figure 1e), consistent with previous reports (Afonina, 2016; Howes, 2016). Malt1 displayed augmented catalytic activity in the presence of CARD14 E138A and CARD14 ΔE138 mutants compared

with WT (Figure 1e). However, CARD14 R38C/E138A lost the ability to stimulate Malt1 activity beyond basal levels. In primary keratinocytes, CARD14 E138A and CARD14 ΔE138 mutants drive production of IL-36γ; however, again

← EYFP-LVSR-eCFP reporter plasmid for 24 hours. (f) Human primary keratinocytes were transfected for 24 hours with Myc-tagged CARD14 constructs. Cell lysates were subject to immunoblotting with anti-Myc, anti-IL-36γ, and anti-β-actin antibodies. Data in a–f are representative of three independent experiments. IB, immunoblot; IP, immunoprecipitation; WT, wild type.

Figure 2. Continued



disruption of the CARD domain abolishes this effect (Figure 1f).

Mutation of Card14 E138 causes spontaneous psoriasiform disease in mice

To define the physiological impact of CARD14 E138 GoF mutation in potentially driving psoriasis pathogenesis, a transgenic mouse incorporating deletion of the E138 residue of CARD14 was generated using CRISPR/Cas9 technology (see Supplementary Figure S2a and b). The *Card14ΔE138* mutation was chosen because it displayed less potent activation of NF-κB, and it was speculated that these mice might be less likely to suffer unwanted defects due to hyperactive NF-κB activity. *Card14ΔE138* heterozygous mice appeared indistinguishable from WT littermates at birth (see Supplementary Figure S2c) but developed dry flaky skin

patches on the back at 5 days of age, which began to disappear at 7 days. However, this progressed to the development of thickened squamous skin on the tail (between 2 and 3 weeks) and, finally, the ears (at 4–5 weeks), reminiscent of human psoriasis skin lesions (see Supplementary Figure S2d and e). Adult mice showed a chronic psoriatic phenotype with thickened squamous skin of the ears and tail and dry skin around the eyes and whiskers, affecting 100% of heterozygous male and female mice (Figure 2a). Ear thickness was significantly increased in *Card14ΔE138^{+/-}* mice compared with WT littermates (Figure 2b). There was no significant difference in weight in *Card14ΔE138^{+/-}* adult mice compared with WT littermates (Figure 2c).

Hematoxylin and eosin staining of ear tissue from *Card14ΔE138^{+/-}* mice showed acanthosis due to keratinocyte hyperproliferation and immune cell infiltration of the

skin (Figure 2d), areas of hyperkeratosis (Figure 2e), including parakeratosis (arrow) and orthokeratosis (arrowhead), and keratotic follicular plugging (see Supplementary Figure S3a online), all hallmarks of human psoriatic skin disease. Similarly, tail skin showed marked hyperplasia (see Supplementary Figure S3b) with increased thickening of the epidermis and immune cell infiltration. In addition to a clear increase in infiltrate of immune cells, the presence of microabscesses was also observed in the epidermis of *Card14ΔE138^{+/-}* mice (Figure 2f). Positive staining with the neutrophil marker Ly6G indicated that neutrophils make up the composition of these microabscesses (Figure 2g). An increased number of enlarged CD31-positive blood vessels were also histologically observed in the dermis, indicating an increase in the dermal vasculature in psoriatic tissue from *Card14ΔE138^{+/-}* mice (Figure 2h, and see Supplementary Figure S3c). In *Card14ΔE138^{+/-}* mice, basal keratinocytes showed strong and abundant expression of the proliferation marker Ki67, indicating hyperproliferation of keratinocytes in the basal layer (Figure 2i, and see Supplementary Figure S3d). Similarly, keratin-14 expression, a marker for the proliferative basal layer of the epidermis, was no longer restricted to basal keratinocytes, as in WT mice, but also present in suprabasal layers, typical of human psoriasis. Expression of keratin-1 (an indicator of early keratinocyte differentiation), which was localized in the suprabasal layer of WT mice, is increased and expressed throughout the epidermis in *Card14ΔE138^{+/-}* mouse skin. *Card14ΔE138* homozygous mice displayed development abnormalities (see Supplementary Figure S4a online) and increased mortality. Surviving neonates were runts (see Supplementary Figure S4b) and died after a few days, typically with a very marked psoriatic phenotype (see Supplementary Figure S4c and d). Toluidine blue staining was performed to determine whether neonates had a skin barrier defect and an increase in skin permeability. Toluidine blue dye failed to stain the epidermis, indicating that neither homozygous nor heterozygous pups had an epidermal barrier defect (see Supplementary Figure S4e).

CARD14 GoF mutation in vivo results in a transcriptomic gene profile similar to human plaque psoriasis

To obtain a comprehensive overview of the transcriptional signature of the inflammatory milieu driving disease pathogenesis in *Card14ΔE138^{+/-}* mice, RNA was extracted from ear tissue of 8-week-old mice and subjected to RNA sequencing analysis (Figure 3a–c). Differentially expressed genes from the psoriatic tissue of *Card14ΔE138^{+/-}* mice included up-regulated hyperproliferative keratins (*Krt6a*, *Krt6b*, *Krt16*); antimicrobial peptides including β -defensins (*Defb3*, *Defb4*, *Defb14*), S100 proteins (*S100a7*, *S100a8*, *S100a9*), and lipocalin-2 (*Lcn2*); and mRNA-encoding cytokines of the innate (IL-1 α , IL-1 β , IL-36 α , IL-36 β , IL-36 γ , IL-6, and IL-17C) and adaptive (IL-20, IL-22, IL-23p19, and IL-17F) immune systems. IL-20 family member IL-19, a cytokine previously shown to be up-regulated in serum and tissue of psoriasis patients and a key component of the IL-23/IL-17A axis, was one of the most highly up-regulated cytokines. IL-19 was shown previously to be specifically expressed by keratinocytes and acts in an autocrine manner in synergy with IL-17A to further enhance induction of anti-bacterial

S100 proteins (Romer et al., 2003; Witte et al., 2014). Up-regulation of chemokines was also evident, including *Ccl20* and the neutrophil chemoattractants *Cxcl1*, *Cxcl2*, *Cxcl3*, and *Cxcl5*. This transcriptional signature likely also reflects secondary changes in dermal endothelial cells and infiltrating immune cells. IL-1 family cytokines, including receptor antagonists, NOD2, caspase-1, caspase-4, and NLRP3, are all up-regulated in *Card14ΔE138^{+/-}* psoriatic tissue, indicating that this phenotype is very much dependent on auto-inflammatory and autoimmunity networks.

Psoriatic tissue from *Card14ΔE138^{+/-}* mice also showed high expression of early cornified envelope proteins including involucrin (*Ivl*) and IL-17A-induced small proline rich proteins (*Sprr2b* and *Sprr2d*). The S100-interacting protein *Fabp5* is also increased. Late cornified envelope proteins including *Lce3b* and *Lce3d* show high expression, and the serine protease inhibitors *Sepinb3a*, *Sepinb3c*, and *Sepina9* are also highly up-regulated. Down-regulated differentially expressed genes include keratin-2 and -24, serpin3b, and serpin12. Filaggrin-2 was also down-regulated, inversely correlating with filaggrin-1 expression in this model. IL-38 (*Ilf10*), an anti-inflammatory cytokine that specifically inhibits IL-36 cytokines, was also down-regulated in *Card14ΔE138^{+/-}* psoriatic tissue, suggesting that in psoriatic skin disease, increased activity of IL-36 cytokines is likely additionally enhanced by decreased expression of this endogenous inhibitor.

We performed pathway analysis and found that *keratinization*, *formation of the cornified envelope*, *signaling by interleukins*, and *antimicrobial peptides* were enriched functions among up-regulated genes (Figure 3c). Comparing transcriptome analysis from *Card14ΔE138^{+/-}* mice with that of human plaque psoriasis available from the publications of Li et al. (2014) (GSE54456) and Keermann et al. (2015) (GSE6651), there is positive enrichment of up-regulated genes with both human studies and negative enrichment of down-regulated genes (Figure 3d). This correlation shows that the transcriptional landscape induced by CARD14 GoF mutation in vivo is typical of human plaque psoriasis.

To further confirm transcriptomic data and to analyze the expression of proinflammatory genes at the onset of macroscopic skin changes in *Card14ΔE138^{+/-}* mice, RNA was extracted from ear tissue of 5-week-old *Card14ΔE138^{+/-}* mice and analyzed by quantitative PCR. Expression of mRNA encoding the proinflammatory cytokines IL-36 γ , IL-1 β , IL-17C, and IL-19 (Figure 3e) was significantly higher in ear tissue of *Card14ΔE138^{+/-}* mice. Similar to human psoriatic skin, *Card14ΔE138^{+/-}* murine tissue showed strong and significantly increased expression of genes encoding the S100 antimicrobial peptides *S100a7* and *S100a8* (Figure 3f); β -defensins *Defb3*, *Defb4*, and *Defb14* (Figure 3g); and the chemokines *Cxcl1*, *Cxcl2*, and *Ccl20* (Figure 3h). Expression of filaggrin-1 and filaggrin-2 was also assessed and confirmed RNA sequencing data, with an increase in filaggrin-1 (*Flg*) and a decrease in filaggrin-2 (*Flg2*) in psoriatic tissue (Figure 3i). Expression of caspase-14, which mediates pro-filaggrin processing to form the cornified envelope, is also increased in *Card14ΔE138^{+/-}* psoriatic tissue (Figure 3a and b). Loss of filaggrin-1 expression is associated with an

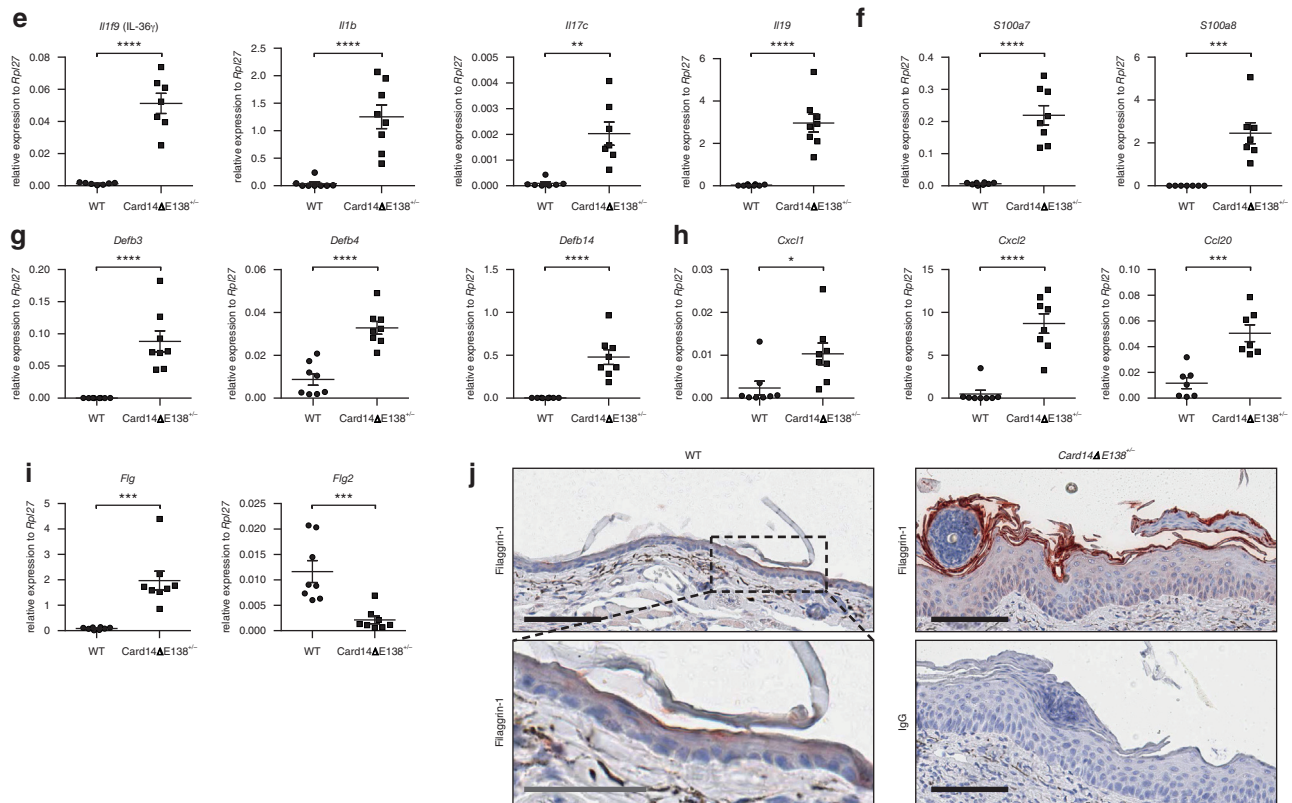


Figure 3. Continued

epidermal barrier dysfunction, which grants microbes the means to invade the epidermis, as in atopic dermatitis (O'Regan et al., 2008). Robust expression of filaggrin-1 in psoriatic tissue of *Card14ΔE138+/-* mice is consistent with the lack of any barrier defect in these mice (Figure 3j).

The CARD14/Bcl10 signaling axis is hyperactive in primary keratinocytes from *Card14ΔE138+/-* mice

To determine whether the epidermal changes observed in *Card14ΔE138+/-* mice were due to dysregulated CARD14 function, epidermal tissue from ear pinnae of WT and *Card14ΔE138+/-* mice were stained for Bcl10 and CARD14 expression. Both molecules showed enhanced expression in the epidermis from *Card14ΔE138+/-* mice compared with WT (Figure 4a). To further assess the CARD14/Bcl10 interaction in *Card14ΔE138+/-* mice, primary keratinocytes were isolated from WT and *Card14ΔE138+/-* mouse epidermis and cultured ex vivo. Murine keratinocytes were subject to lysis in Triton X-100-containing lysis buffer and soluble and insoluble fractions subject to SDS-PAGE (Figure 4b). CARD14 and Bcl10 showed increased expression in the insoluble fraction in *Card14ΔE138+/-*-derived cells compared with WT control

cells, which correlated with decreased expression in the soluble fraction. Additionally, Bcl10 and CARD14 showed increased interaction as determined by co-immunoprecipitation (Figure 4c) and enhanced processing of Malt1 substrate protein RelB. Bcl10 expression was visualized by confocal microscopy, and in primary keratinocytes from WT mice, Bcl10 was expressed uniformly throughout the cytoplasm; however, in keratinocytes from *Card14ΔE138+/-* mice Bcl10 was observed in discrete signalosome structures (Figure 4d). To assess the downstream effects of this increased interaction, transcript levels of pro-inflammatory molecules were assessed in keratinocytes isolated and cultured from WT and *Card14ΔE138+/-* mouse epidermis by quantitative PCR. Levels of mRNA encoding S100A7, IL-17C, IL-19, and IL-36γ were significantly increased in *Card14ΔE138+/-* keratinocytes compared with WT cells (Figure 4e).

Neutralization of the T helper type 17-polarizing cytokine IL-23 p19 subunit attenuates disease symptoms

We next characterized the immune infiltrate of the skin of *Card14ΔE138+/-* mice. Psoriatic skin of *Card14ΔE138+/-*

overlap between the pathway and the gene set. The color represents the *P*-value. (d) Gene set enrichment analysis enrichment plots comparing transcriptome data from *Card14ΔE138+/-* mice with online published data from human plaque psoriasis patients, GSE66511 and GSE54456. Normalized enrichment score (NES) and adjusted *P*-value (padj) are indicated. (e–i) RNA was extracted from whole ear tissue of 5-week-old mice and subjected to quantitative PCR analysis to measure mRNA expression levels of (e) *Il1f9* (IL-36γ), *Il1b*, *Il17c*, and *Il19*; (f) *S100a7* and *S100a8*; (g) *Defb3*, *Defb4*, and *Defb14*; (h) *Cxcl1*, *Cxcl2*, and *Ccl20*; and (i) *Flg* and *Flg2*. (j) Ear sections from 8-week-old *Card14ΔE138+/-* and wild-type littermates were stained with a specific antibody against filaggrin-1 or isotype control. Black scale bar = 100 μm; gray scale bar = 50 μm. (a–d) Analysis of one experiment with three mice per group; (e–i) representative of two independent experiments with seven or eight mice per group (total *n* = 15), and data were subjected to a two-tailed unpaired Student *t* test. **P* < 0.05, ***P* < 0.01, ****P* < 0.001, *****P* < 0.0001. (j) Representative of eight individual mice per group. DEGs, differentially expressed genes; WT, wild type.

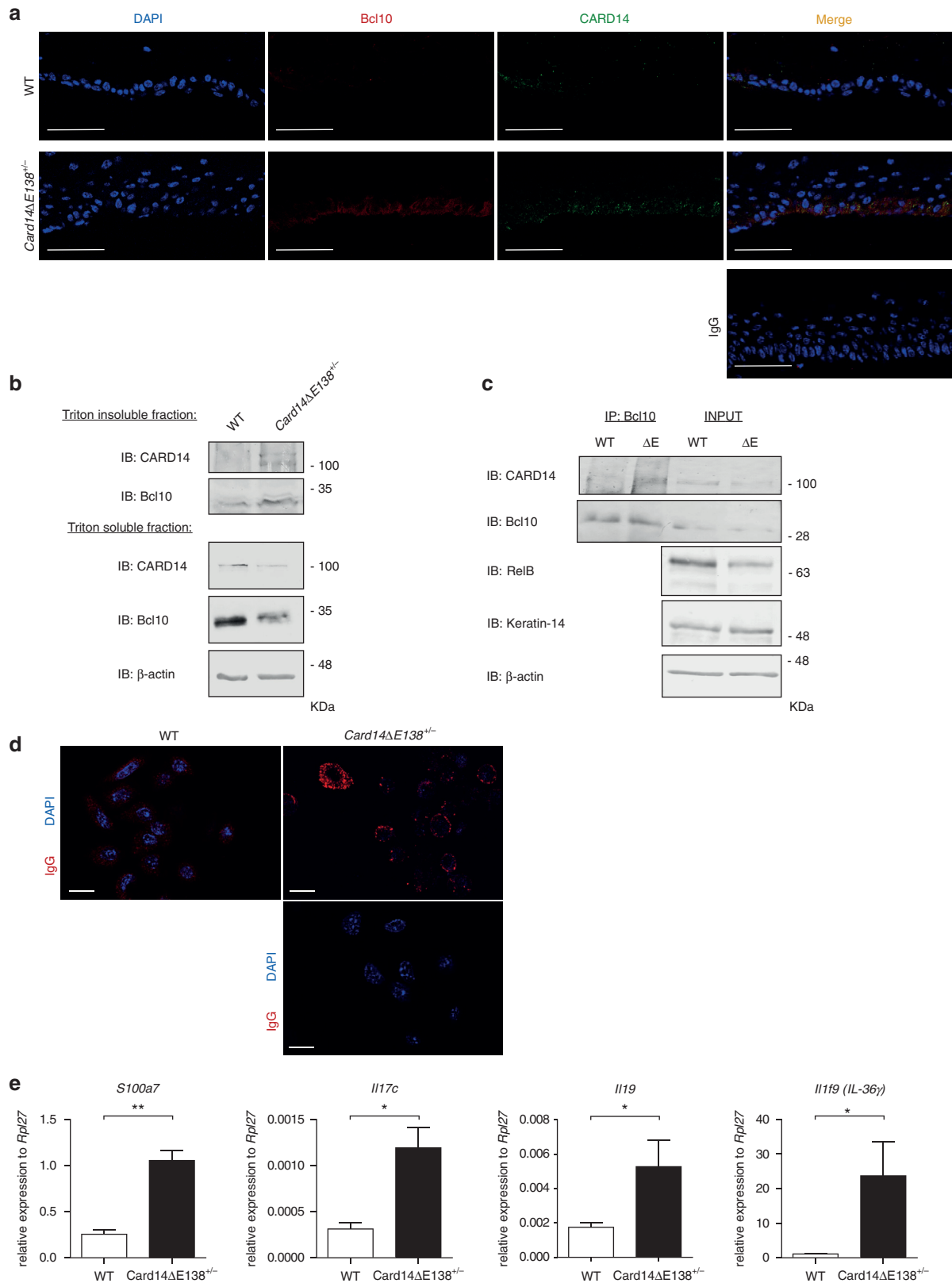


Figure 4. Keratinocytes from *Card14ΔE138^{+/-}* mice display enhanced CARD14/Bcl10 activity. (a) Confocal microscopy analysis of epidermal tissue from ear pinnae from WT and *Card14ΔE138^{+/-}* mice stained for specific anti-Bcl10, -CARD14, or isotype control antibodies. Nuclei were stained with DAPI. Scale bar = 50 μm. (b–e) Primary murine keratinocytes were isolated from WT and *Card14ΔE138^{+/-}* tail epidermis and cultured ex vivo for 3–4 days. (b) Cells were lysed in Triton-X–containing buffer, and soluble and insoluble fractions were subject to SDS-PAGE followed by immunoblotting with indicated antibodies. (c) Cell lysates were immunoprecipitated with an anti-Bcl10 antibody, followed by immunoblotting with indicated antibodies. ΔE = keratinocytes from *Card14ΔE138^{+/-}* mice. (d) Cells visualized for expression and localization of endogenous murine Bcl10 by confocal microscopy using a specific anti-Bcl10 antibody. Nuclei were stained with DAPI. Scale bar = 15 μm. (e) RNA was extracted from whole ear tissue of 5-week-old mice and subjected to quantitative PCR

mice harbors a pronounced infiltrate of CD45-positive leukocytes (Figure 5a). This immune infiltrate is composed of increased numbers of neutrophils, myeloid antigen-presenting cells, and $\gamma\delta$ and $\alpha\beta$ T cells compared with WT littermates (Figure 5b, and see Supplementary Figure S5 online). T helper (Th) 17 cells play a central role in psoriasis pathogenesis, and IL-23 maintains the differentiation of pathogenic Th17 cells, which secrete IL-17A and IL-22, two of the cytokines that mediate the inflammatory effects and hyperproliferation associated with human psoriasis (Cai et al., 2012). Indeed, protein levels of IL-17A and IL-22 were significantly increased in *Card14 Δ E138^{+/-}* ear tissue of adult mice (Figure 5c). IL-23p19, IL-17A, and IL-22—encoding transcripts were also seen at significantly higher levels in 5-week-old *Card14 Δ E138^{+/-}* mouse skin (Figure 5d). Similarly, the Th1 cytokines IFN γ and TNF- α were also significantly elevated in ear tissue of 5-week-old *Card14 Δ E138^{+/-}* mice (Figure 5e), contributing to an inflammatory milieu typical of human psoriasis.

To assess whether CARD14-induced psoriatic disease symptoms can be attenuated in vivo by targeted disruption of the IL-23/Th17 axis, *Card14 Δ E138^{+/-}* heterozygous mice were treated with a neutralizing antibody specific for the murine IL-23p19 subunit by intraperitoneal injection over the course of 15 days, and control mice were administered an IgG isotype antibody. Mice receiving anti-IL-23p19—neutralizing antibody showed a significantly decreased psoriatic phenotype on the ears and tail after 2 weeks of therapy (Figure 5f) and a significant reduction in ear thickness versus at the onset of treatment and versus IgG control animals (Figure 5g). Further reductions were evident after administration of IL-23p19 over 3 weeks (see Supplementary Figure S6a–c online). Histological features were assessed by the scoring system of Baker et al. (1992), and IL-23p19—treated mice showed a significant decrease in murine clinical score (Figure 5h and i). In vivo blockade of IL-23p19 also reduced expression of mRNA encoding β -defensins, S100 proteins, IL-36 γ , and IL-19 (Figure 5j). These results indicate that disruption of the IL-23/Th17 immune signaling axis is sufficient to reverse the aberrant epidermal signaling networks induced by CARD14 GoF mutation. Thus, CARD14 GoF drives IL-23—mediated psoriatic skin disease, and targeting of IL-23p19 in this mouse model is a rapid and effective therapeutic option, consistent with reports from phase III clinical trials in patients with plaque-type psoriasis (Nakamura et al., 2017; Papp et al., 2017; Reich et al., 2017).

DISCUSSION

Psoriasis is a common but complex inflammatory skin disease that arises from the interplay between stress or trauma within the epidermis and a dysregulated immune response. Genetic studies have shown a role for selected genes, particularly those of the innate and adaptive immune system and the IL-23/IL-17 signaling axis (Tsoi, 2012). Several genes encoding proteins in epithelial barrier function have also been linked to psoriasis susceptibility, and GoF mutations in

the gene encoding the keratinocyte signaling molecule, CARD14, have been associated with both psoriasis and PRP, although the extent to which CARD14 genetic variants contribute to disease susceptibility is currently unclear.

Here, we unequivocally show that CARD14 GoF alone is sufficient to drive disease pathogenesis in vivo and show that a single amino acid mutation of a key glutamic acid (E138) results in the complete immunological and clinical phenotype of plaque-type psoriasis in mice. The etiology of psoriasis has been elusive in the past, regarding the contribution of keratinocyte dysfunction versus altered immune function (Bos et al., 2005; Christophers, 1996). However, our data strongly suggest that dysregulated keratinocyte signaling pathways initiated by CARD14 contribute to drive the pathogenic IL-23/IL-17 axis in vivo. *Card14 Δ E138* heterozygous mice spontaneously and rapidly developed a chronic psoriatic phenotype with scaling skin lesions, epidermal acanthosis, parakeratosis, and hyperkeratosis, keratinocyte hyperproliferation, and immune cell infiltration of lesional skin. In addition to *Card14 Δ E138^{+/-}* tissue recapitulating the histological features of psoriasis, transcriptome profiling from affected skin in these mice correlated with up-regulated and down-regulated gene signatures observed in human plaque psoriasis. In particular, high expression of antimicrobial peptides (β -defensins, S100 proteins), chemokines (*Cxcl2*, *Ccl20*), and cytokines (including IL-19, IL-36 γ , IL-1 β , and IL-23p19) were observed. Additionally, neutralization of IL-23p19 significantly reduced skin lesions and the expression of anti-microbial peptides and proinflammatory cytokines in the skin of *Card14 Δ E138* mice.

Tanaka et al. (2018) recently showed that CARD14-deficient mice were protected from developing imiquimod-induced psoriasisiform disease (Tanaka et al., 2018), which is consistent with our results that GoF mutation in CARD14 is sufficient to drive the complete immunopathogenesis of psoriatic disease in vivo. Tanaka's study shows a role for CARD14-positive hematopoietic cells in imiquimod-induced psoriasisiform disease. In our study, keratinocytes harboring mutant CARD14 contribute to disease pathogenesis; however, it will be of interest to further tease out the interplay of these different cell types in disease pathogenesis. Taken together, these reports place CARD14 in a central role of mediating psoriatic skin disease pathogenesis, which warrants further clinical appraisal. The physiological relevance to human disease means that the *Card14 Δ E138^{+/-}* mouse model will become an invaluable tool for dissecting the complex signaling networks associated with psoriatic skin disease. This model will also be beneficial in the preclinical assessment of therapeutics aimed at specifically targeting molecular drivers of psoriasis and PRP in the future. These findings highlight the formation of the CARD14/Bcl10/Malt1 complex as a key cellular process to target in the development of future therapies for psoriatic disease. Malt1-specific inhibitors have been suggested as a potential therapeutic strategy that can be used for treating psoriatic skin disease, because inhibition of Malt1 function would have the benefit

analysis of mRNA expression of *S100a7*, *Il17c*, *Il19*, and *Il1f9* (IL-36 γ). (a–d) Images are representative of three independent experiments or (e) data are presented as the mean \pm standard error of the mean of three independent experiments and were subjected to a two-tailed unpaired Student *t* test. **P* < 0.05, ***P* < 0.01. IB, immunoblot; WT, wild type.

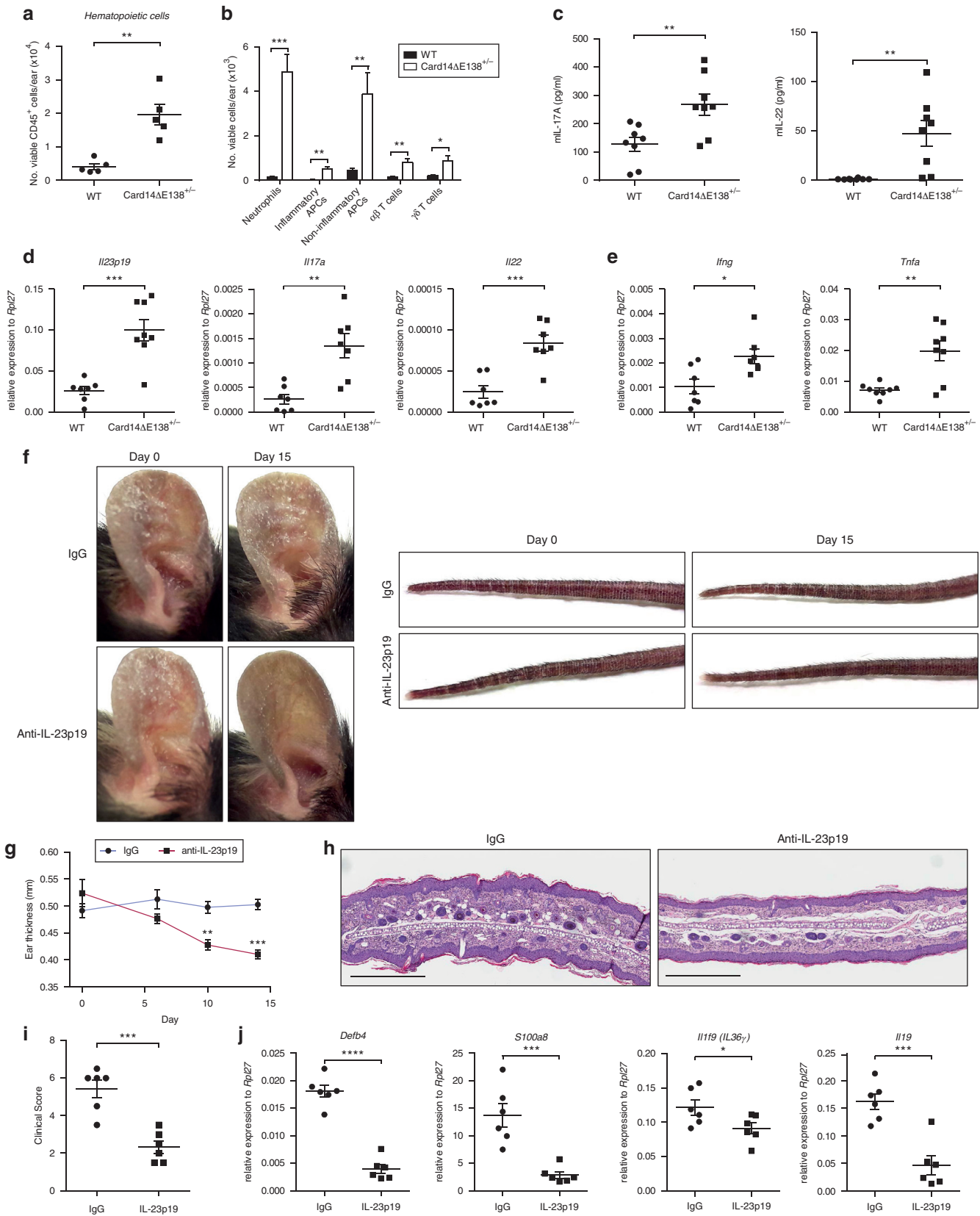


Figure 5. Immune cell infiltrate shows a T helper type 17 signature, and IL-23p19 neutralization ameliorates the phenotype in *Card14ΔE138^{+/-}* mice. (a, b) Flow cytometry analysis of single-cell suspension from ear tissue from age- and sex-matched adult *Card14ΔE138^{+/-}* mice and littermate controls. Shown are the number of (a) CD45⁺ hematopoietic cells and (b) neutrophils (CD11b⁺Ly6G⁺), inflammatory (CD11b⁺Ly6G⁻NK1.1⁻MHCII^{hi}Ly6C^{hi}) and noninflammatory (CD11b⁺Ly6G⁻NK1.1⁻MHCII^{lo}Ly6C⁻) APCs, αβ T cells (CD3^{low}TCRβ⁺), and γδ T cells (CD3^{low}TCRβ⁺) per ear. (c) Whole ears from age- and sex-matched adult *Card14ΔE138^{+/-}* and wild-type mice were homogenized and analyzed for IL-17A and IL-22 protein levels by ELISA (n = 8). (d, e) RNA was extracted from whole ear tissue of 5-week-old mice and subjected to quantitative PCR analysis of (d) *Il23p19*, *Il17a*, and *Il22* or (e) *Ifng* (IFNγ) and *Tnfa* mRNA expression

of affecting T-cell and keratinocyte function (downstream of CARD11 and CARD14, respectively) (Van Nuffel et al., 2017). Targeting CARD14 directly, however, may permit the development of more specific therapies with decreased adverse effect profiles, and this merits further investigation into understanding CARD14 biology.

MATERIALS AND METHODS

Details of the materials and methods are given in the [Supplementary Materials](#) online.

Genetically modified mouse strains

To generate *Card14ΔE138* mice, C57BL/6J (JR 000664) oocytes were microinjected with Cas9 mRNA and donor DNA along with one of two guide RNA sequences. Two strains harboring the *Card14ΔE138* deletion were generated from separate founder animals, strains 28900 (C57BL/6J-Card14em9(delE138)Lutzyl) and 28882 (C57BL/6J-Card14em5(delE138)Lutzyl). Mouse strain 28900 was used for the experiments described in the article. All animal experiments were performed in accordance with the regulations and guidelines of and with ethical approval from the Cantonal Veterinary Office of Zürich, Switzerland.

Cell culture

Human primary keratinocytes were cultured as previously described (Feldmeyer et al., 2007). Briefly, human primary foreskin keratinocytes were passaged in keratinocyte serum-free medium (Thermo Fisher Scientific, Waltham, MA), supplemented with epithelial growth factor and bovine pituitary extract (Thermo Fisher Scientific), and seeded for experiments after 3 passages. All cells were maintained at 37 °C in a humidified atmosphere of 5% CO₂.

RNA sequencing transcriptome analysis

RNA was extracted from whole ear tissue from 8-week-old female WT and *Card14ΔE138*^{+/-} mice. After library preparation, samples were analyzed with the Illumina HiSeq 4000 (Illumina, San Diego, CA), which was used to generate single end reads of length 125 nucleotides. For data processing, the raw reads were first cleaned by removing adapter sequences, trimming low-quality ends, and filtering reads with low quality (phred quality < 20) using Trimmomatic (Bolger et al., 2014). Sequence alignment of the resulting high-quality reads to the *Mus musculus* reference genome (build GRCh38) and quantification of gene level expression was carried out using RSEM, version 1.3.0 (Li and Dewey, 2011). Differential expression was computed using the generalized linear model implemented in the Bioconductor package EdgeR, version 3.20.1 (Robinson et al., 2010). The data was deposited in the European Nucleotide Archive (accession number PRJEB25394). Pathway analysis was performed using ReactomePA (Yu and He, 2016). The top significant pathways were plotted as a dotplot. Gene set enrichment analysis was performed using fgsea (Sergushichev, 2016), and datasets from GSE66511 and

GSE54456 were obtained from the National Center for Biotechnology Information Gene Expression Omnibus.

ORCID

Mark Mellett: <http://orcid.org/0000-0002-6315-167X>

CONFLICT OF INTEREST

The authors state no conflict of interest.

ACKNOWLEDGMENTS

The authors thank D. Kazakov, L. Opitz, M. Comazzi, B. Henriques, C. Décaillet, E. Härtel, T. Koch, E. Guenova, G. Fenini, S. Grossi, and H.D. Beer for technical assistance and expertise and Burkhard Becher (University of Zürich), Jeremy Di Domizio, and Michel Gilliet (University Hospital of Lausanne, CHUV) for critical analysis of the manuscript. MM thanks the University of Zürich Forschungskredit, the Swiss Life Jubiläumstiftung, the European Union-funded Marie Skłodowska-Curie Individual Fellowship for financial support, and the Rare Genomics Institute BeHEARD Science Challenge and the Jackson Laboratories (particularly A. Zuberi and C. Lutz) for the generation of the *Card14ΔE138* mouse strains. MT acknowledges support from the Swiss National Science Foundation and the Emma Muschamp Foundation. EC and LEF are supported by grants from the Swiss National Science Foundation (grant number 310030-156384) and Zürich University Research Priority Program (URPP) Translational Cancer Research.

AUTHOR CONTRIBUTIONS

MM conceived the study and mouse models, developed the concept, designed and performed experiments, analyzed the data, co-supervised the project and wrote the manuscript. BM designed and performed immunohistochemistry experiments and analysis. DM performed flow cytometry and analysis. RS performed the fluorescence resonance energy transfer assay and subsequent flow cytometry, immunoblotting and data analysis. PC analyzed the RNA sequencing transcriptomic data, BK performed immunohistochemistry experiments, TS and SN contributed critical analysis and experimental design. MT and EC designed experiments, provided critical analysis of data and the manuscript. LEF supervised the project, provided critical analysis of data and co-wrote the manuscript.

SUPPLEMENTARY MATERIAL

Supplementary material is linked to the online version of the paper at www.jidonline.org, and at <https://doi.org/10.1016/j.jid.2018.03.1525>.

REFERENCES

- Afonina IS, Van Nuffel E, Baudelet G, Driege Y, Kreike M, Staal J, et al. The paracaspase MALT1 mediates CARD14-induced signaling in keratinocytes. *EMBO Rep* 2016;17:914–27.
- Baker BS, Brent L, Valdimarsson H, Powles AV, al-Imara L, Walker M, et al. Is epidermal cell proliferation in psoriatic skin grafts on nude mice driven by T-cell derived cytokines? *Br J Dermatol* 1992;126:105–10.
- Berki DM, Liu L, Choon SE, David Burden A, Griffiths CEM, Navarini AA, et al. Activating CARD14 mutations are associated with generalized pustular psoriasis but rarely account for familial recurrence in psoriasis vulgaris. *J Invest Dermatol* 2015;135:2964–70.
- Bertin J, Wang L, Guo Y, Jacobson MD, Poyet JL, Srinivasula SM, et al. CARD11 and CARD14 are novel caspase recruitment domain (CARD)/membrane-associated guanylate kinase (MAGUK) family members that interact with BCL10 and activate NF-kappa B. *J Biol Chem* 2001;276:11877–82.
- Bolger AM, Lohse M, Usadel B. Trimmomatic: a flexible trimmer for Illumina sequence data. *Bioinformatics* 2014;30:2114–20.
- Bos JD, De Rie MA. The pathogenesis of psoriasis: immunological facts and speculations. *Immunol Today* 1999;20:40–6.

levels. (f) Macroscopic images of ears and tails of IgG- and IL-23p19–treated mice at the beginning and end (day 15) of the experiment. (g) Ear thickness of IL-23p19–treated animals and control animals at days 0, 6, 10, and 15 of the experiment. IL-23p19 group, n = 6; IgG group, n = 6. (h) Representative histological features shown by hematoxylin and eosin staining at day 15. Scale bar = 500 μm. (i) Clinical scoring of histological features of IgG- versus IL-23p19–treated mice. (j) quantitative PCR analysis of mRNA expression of *Defb4*, *S100a8*, *Il1f9* (IL-36γ), and *Il19* in ear tissue from IL-23p19–treated and IgG-treated mice. Data are representative of (a, b) three independent experiments, (c) one experiment with eight or nine mice per group, or (d, e) two independent experiments with seven or eight mice per group. Total n = 15. (f) Images are representative of IgG- and IL-23p19–treated mice (total n = 10 per group) or (g–j) data are presented as the mean ± standard error of the mean of six mice, representative of two independent experiments (total n = 10 per group) and were subjected to a two-tailed unpaired Student *t* test. **P* < 0.05, ***P* < 0.01, ****P* < 0.001, *****P* < 0.0001. APC, antigen-presenting cell; WT, wild type.

- Bos JD, de Rie MA, Teunissen MB, Piskin G. Psoriasis: dysregulation of innate immunity. *Br J Dermatol* 2005;152:1098–107.
- Boyman O, Conrad C, Tonel G, Gilliet M, Nestle FO. The pathogenic role of tissue-resident immune cells in psoriasis. *Trends Immunol* 2007;28:51–7.
- Cai Y, Fleming C, Yan J. New insights of T cells in the pathogenesis of psoriasis. *Cell Mol Immunol* 2012;9:302–9.
- Christophers E. The immunopathology of psoriasis. *Int Arch Allergy Immunol* 1996;110:199–206.
- Christophers E. Psoriasis—epidemiology and clinical spectrum. *Clin Exp Dermatol* 2001;26:314–20.
- Du S, Jia L, Zhang Y, Fang L, Zhang X, Fan Y. CARMA3 is upregulated in human pancreatic carcinoma, and its depletion inhibits tumor proliferation, migration, and invasion. *Tumour Biol* 2014;35:5965–70.
- Feldmeyer L, Keller M, Niklaus G, Hohl D, Werner S, Beer HD. The inflammasome mediates UVB-induced activation and secretion of interleukin-1beta by keratinocytes. *Curr Biol* 2007;17:1140–5.
- Fuchs-Telem D, Sarig O, van Steensel MA, Isakov O, Israeli S, Nussbeck J, et al. Familial pityriasis rubra pilaris is caused by mutations in CARD14. *Am J Hum Genet* 2012;91:163–70.
- Gaide O, Favier B, Legler DF, Bonnet D, Brissoni B, Valitutti S, et al. CARMA1 is a critical lipid raft-associated regulator of TCR-induced NF-kappa B activation. *Nat Immunol* 2002;3:836–43.
- Gaide O, Martinon F, Micheau O, Bonnet D, Thome M, Tschopp J. Carma1, a CARD-containing binding partner of Bcl10, induces Bcl10 phosphorylation and NF-kappaB activation. *FEBS Lett* 2001;496(2-3):121–7.
- Griffiths CE, Barker JN. Pathogenesis and clinical features of psoriasis. *Lancet* 2007;370(9583):263–71.
- Gudjonsson JE, Elder JT. Psoriasis: epidemiology. *Clin Dermatol* 2007;25:535–46.
- Harden JL, Lewis SM, Pierson KC, Suarez-Farinas M, Lentini T, Ortenzio FS, et al. CARD14 expression in dermal endothelial cells in psoriasis. *PLoS One* 2014;9(11):e111255.
- Has C, Schwieger-Briel A, Schlipf N, Hausser I, Chmel N, Rosler B, et al. Target-sequence capture and high throughput sequencing identify a de novo CARD14 mutation in an infant with erythrodermic pityriasis rubra pilaris. *Acta Derm Venereol* 2016;96:989–90.
- Hong JB, Chen PL, Chen YT, Tsai TF. Genetic analysis of CARD14 in non-familial pityriasis rubra pilaris: a case series. *Acta Derm Venereol* 2014;94:587–8.
- Howes A, O'Sullivan PA, Breyer F, Ghose A, Cao L, Krappmann D, et al. Psoriasis mutations disrupt CARD14 autoinhibition promoting BCL10-MALT1-dependent NF-kappaB activation. *Biochem J* 2016;473:1759–68.
- Inoue N, Dainichi T, Fujisawa A, Nakano H, Sawamura D, Kabashima K. CARD14 Glu138 mutation in familial pityriasis rubra pilaris does not warrant differentiation from familial psoriasis. *J Dermatol* 2016;43:187–9.
- Jattani RP, Tritapoe JM, Pomerantz JL. Cooperative control of caspase recruitment domain-containing protein 11 (CARD11) signaling by an unusual array of redundant repressive elements. *J Biol Chem* 2016;291:8324–36.
- Jordan CT, Cao L, Roberson ED, Duan S, Helms CA, Nair RP, et al. Rare and common variants in CARD14, encoding an epidermal regulator of NF-kappaB, in psoriasis. *Am J Hum Genet* 2012a;90:796–808.
- Jordan CT, Cao L, Roberson ED, Pierson KC, Yang CF, Joyce CE, et al. PSORS2 is due to mutations in CARD14. *Am J Hum Genet* 2012b;90:784–95.
- Juillard M, Thome M. Role of the CARMA1/BCL10/MALT1 complex in lymphoid malignancies. *Curr Opin Hematol* 2016;23:402–9.
- Keermann M, Koks S, Reimann E, Prans E, Abram K, Kingo K. Transcriptional landscape of psoriasis identifies the involvement of IL36 and IL36RN. *BMC Genomics* 2015;16:322.
- Li B, Dewey CN. RSEM: accurate transcript quantification from RNA-seq data with or without a reference genome. *BMC Bioinformatics* 2011;12:323.
- Li B, Tsoi LC, Swindell WR, Gudjonsson JE, Tejasvi T, Johnston A, et al. Transcriptome analysis of psoriasis in a large case-control sample: RNA-seq provides insights into disease mechanisms. *J Invest Dermatol* 2014;134:1828–38.
- Li Q, Jin Chung H, Ross N, Keller M, Andrews J, Kingman J, et al. Analysis of CARD14 polymorphisms in pityriasis rubra pilaris: activation of NF-kappaB. *J Invest Dermatol* 2015;135:1905–8.
- McAllister-Lucas LM, Inohara N, Lucas PC, Ruland J, Benito A, Li Q, et al. Bimp1, a MAGUK family member linking protein kinase C activation to Bcl10-mediated NF-kappaB induction. *J Biol Chem* 2001;276:30589–97.
- Mease PJ, Gladman DD, Papp KA, Khraishi MM, Thaci D, Behrens F, et al. Prevalence of rheumatologist-diagnosed psoriatic arthritis in patients with psoriasis in European/North American dermatology clinics. *J Am Acad Dermatol* 2013;69:729–35.
- Mossner R, Frambach Y, Wilsmann-Theis D, Lohr S, Jacobi A, Weyergraf A, et al. Palmoplantar pustular psoriasis is associated with missense variants in CARD14, but not with loss-of-function mutations in IL36RN in European patients. *J Invest Dermatol* 2015;135:2538–41.
- Nakamura M, Lee K, Jeon C, Sekhon S, Afifi L, Yan D, et al. Guselkumab for the treatment of psoriasis: a review of phase III trials. *Dermatol Ther (Heidelb)* 2017;7:281–92.
- O'Regan GM, Sandilands A, McLean WH, Irvine AD. Filaggrin in atopic dermatitis. *J Allergy Clin Immunol* 2008;122:689–93.
- Pan D, Zhu Y, Zhou Z, Wang T, You H, Jiang C, et al. The CBM complex underwrites NF-kappaB activation to promote HER2-associated tumor malignancy. *Mol Cancer Res* 2016;14:93–102.
- Papp KA, Blauvelt A, Bukhalo M, Gooderham M, Krueger JG, Lacour JP, et al. Risankizumab versus ustekinumab for moderate-to-severe plaque psoriasis. *N Engl J Med* 2017;376:1551–60.
- Pelzer C, Cabalzar K, Wolf A, Gonzalez M, Lenz G, Thome M. The protease activity of the paracaspase MALT1 is controlled by monoubiquitination. *Nat Immunol* 2013;14:337–45.
- Pomerantz JL, Denny EM, Baltimore D. CARD11 mediates factor-specific activation of NF-kappaB by the T cell receptor complex. *EMBO J* 2002;21:5184–94.
- Qiao Q, Yang C, Zheng C, Fontan L, David L, Yu X, et al. Structural architecture of the CARMA1/Bcl10/MALT1 signalosome: nucleation-induced filamentous assembly. *Mol Cell* 2013;51:766–79.
- Reich K, Papp KA, Blauvelt A, Tying SK, Sinclair R, Thaci D, et al. Tildrakizumab versus placebo or etanercept for chronic plaque psoriasis (reSURFACE 1 and reSURFACE 2): results from two randomised controlled, phase 3 trials. *Lancet* 2017;390(10091):276–88.
- Robinson MD, McCarthy DJ, Smyth GK. edgeR: a Bioconductor package for differential expression analysis of digital gene expression data. *Bioinformatics* 2010;26:139–40.
- Romer J, Hasselager E, Norby PL, Steiniche T, Thorn Clausen J, Kragballe K. Epidermal overexpression of interleukin-19 and -20 mRNA in psoriatic skin disappears after short-term treatment with cyclosporine a or calcipotriol. *J Invest Dermatol* 2003;121:1306–11.
- Sano S, Chan KS, Carbajal S, Clifford J, Peavey M, Kiguchi K, et al. Stat3 links activated keratinocytes and immunocytes required for development of psoriasis in a novel transgenic mouse model. *Nat Med* 2005;11:43–9.
- Schmitt A, Grondona P, Maier T, Brandle M, Schonfeld C, Jager G, et al. MALT1 protease activity controls the expression of inflammatory genes in keratinocytes upon zymosan stimulation. *J Invest Dermatol* 2016;136:788–97.
- Scudiero I, Mazzone P, D'Andrea LE, Ferravante A, Zotti T, Telesio G, et al. CARMA2sh and ULK2 control pathogen-associated molecular patterns recognition in human keratinocytes: psoriasis-linked CARMA2sh mutants escape ULK2 censorship. *Cell Death Dis* 2017;8(2):e2627.
- Scudiero I, Vito P, Stilo R. The three CARMA sisters: so different, so similar: a portrait of the three CARMA proteins and their involvement in human disorders. *J Cell Physiol* 2014;229:990–7.
- Scudiero I, Zotti T, Ferravante A, Vessichelli M, Vito P, Stilo R. Alternative splicing of CARMA2/CARD14 transcripts generates protein variants with differential effect on NF-kappaB activation and endoplasmic reticulum stress-induced cell death. *J Cell Physiol* 2011;226:3121–31.
- Sergushichev A. An algorithm for fast preranked gene set enrichment analysis using cumulative statistic calculation. *bioRxiv* 2016. <https://doi.org/10.1101/060012>. Accessed 28 May 2018.
- Sheng Y, Jin X, Xu J, Gao J, Du X, Duan D, et al. Sequencing-based approach identified three new susceptibility loci for psoriasis. *Nat Commun* 2014;5:4331.
- Sugiura K, Muto M, Akiyama M. CARD14 c.526G>C (p.Asp176His) is a significant risk factor for generalized pustular psoriasis with psoriasis vulgaris in the Japanese cohort. *J Invest Dermatol* 2014;134:1755–7.
- Takeichi T, Kobayashi A, Ogawa E, Okuno Y, Kataoka S, Kono M, et al. Autosomal dominant familial generalized pustular psoriasis caused by a CARD14 mutation. *Br J Dermatol* 2017;177:e133–5.

- Takeichi T, Sugiura K, Nomura T, Sakamoto T, Ogawa Y, Oiso N, et al. Pityriasis rubra pilaris type V as an autoinflammatory disease by CARD14 mutations. *JAMA Dermatol* 2017;153:66–70.
- Tanaka M, Kobiyama K, Honda T, Uchio-Yamada K, Natsume-Kitatani Y, Mizuguchi K, et al. Essential role of CARD14 in murine experimental psoriasis. *J Immunol* 2018;200:71–81.
- Tsoi LC, Spain SL, Knight J, Ellinghaus E, Stuart PE, Capon F, et al. Identification of 15 new psoriasis susceptibility loci highlights the role of innate immunity. *Nat Genet* 2012;44:1341–8.
- Tsoi LC, Stuart PE, Tian C, Gudjonsson JE, Das S, Zawistowski M, et al. Large scale meta-analysis characterizes genetic architecture for common psoriasis associated variants. *Nat Commun* 2017;8:15382.
- Valdimarsson H, Baker BS, Jonsdottir I, Powles A, Fry L. Psoriasis: a T-cell-mediated autoimmune disease induced by streptococcal superantigens? *Immunol Today* 1995;16:145–9.
- Van Nuffel E, Schmitt A, Afonina IS, Schulze-Osthoff K, Beyaert R, Hailfinger S. CARD14-mediated activation of paracaspase MALT1 in keratinocytes: implications for psoriasis. *J Invest Dermatol* 2017;137:569–75.
- Wang D, You Y, Case SM, McAllister-Lucas LM, Wang L, DiStefano PS, et al. A requirement for CARMA1 in TCR-induced NF-kappa B activation. *Nat Immunol* 2002;3:830–5.
- Witte E, Kokolakis G, Witte K, Philipp S, Doecke WD, Babel N, et al. IL-19 is a component of the pathogenetic IL-23/IL-17 cascade in psoriasis. *J Invest Dermatol* 2014;134:2757–67.
- Xia ZX, Li ZX, Zhang M, Sun LM, Zhang QF, Qiu XS. CARMA3 regulates the invasion, migration, and apoptosis of non-small cell lung cancer cells by activating NF-κB and suppressing the P38 MAPK signaling pathway. *Exp Mol Pathol* 2016;100:353–60.
- Xie C, Han Y, Fu L, Li Q, Qiu X, Wang E. Overexpression of CARMA3 is associated with advanced tumor stage, cell cycle progression, and cisplatin resistance in human epithelial ovarian cancer. *Tumour Biol* 2014;35:7957–64.
- Yu G, He QY. ReactomePA: an R/Bioconductor package for reactome pathway analysis and visualization. *Mol Biosyst* 2016;12:477–9.



This work is licensed under a Creative Commons Attribution-NonCommercial-NoDerivatives 4.0 International License. To view a copy of this license, visit <http://creativecommons.org/licenses/by-nc-nd/4.0/>